PCCP

PAPER

View Article Online
View Journal | View Issue

Cite this: *Phys. Chem. Chem. Phys.*, 2017, **19**, 19243

Oxygen storage properties of hexagonal $HoMnO_{3+\delta}$†

Konrad Świerczek,[ab] Alicja Klimkowicz, *[c] Kengo Nishihara,[c] Shuntaro Kobayashi,[c] Akito Takasaki,[c] Maleeha Alanizy,[d] Stanislaw Kolesnik,[d] Bogdan Dabrowski,[d] Seungho Seong[e] and Jeongsoo Kang[e]

Structural and oxygen content changes of hexagonal $HoMnO_{3+\delta}$ manganite at the stability boundary in the perovskite phase have been studied by X-ray diffraction and thermogravimetry using *in situ* oxidation and reduction processes at elevated temperatures in oxygen and air. The oxygen storage properties during structural transformation between stoichiometric Hex0 and oxygen-loaded Hex1 phases, transition temperatures and kinetics of the oxygen incorporation and release are reported for materials prepared by the solid-state synthesis and high-impact mechanical milling. Long-term annealing experiments have shown that the Hex0 (δ = 0) → Hex1 ($\delta \approx 0.28$) phase transition is limited by the surface reaction and nucleation of the new phase for $HoMnO_{3+\delta}$ 15MM. The temperatures of Hex0 ↔ Hex1 transitions have been established at 290 °C and 250 °C upon heating and cooling, respectively, at a rate of 0.1° min^{-1}, also indicating that the temperature hysteresis of the transition could possibly be as small as 10 °C in the equilibrium. Ball-milling of $HoMnO_{3+\delta}$ has only a small effect on improving the speed of the reduction/oxidation processes in oxygen, but importantly, allowed for considerable oxygen incorporation in air at a temperature range of 220–255 °C after prolonged heating. The Mn 2p XAS results of the Mn valence in oxygen loaded samples support the oxygen content determined by the TG method. The magnetic susceptibility data of the effective Mn valence gave inconclusive results due to dominating magnetism of the Ho^{3+} ions. Comparison of $HoMnO_{3+\delta}$ with previously studied $DyMnO_{3+\delta}$ indicates that a tiny increase in the ionic size of lanthanide has a huge effect on the redox properties of hexagonal manganites and that practical properties could be significantly improved by synthesizing the larger average size $(Y,Ln)MnO_{3+\delta}$ manganites.

Received 26th May 2017,
Accepted 26th June 2017

DOI: 10.1039/c7cp03556j

rsc.li/pccp

1. Introduction

Usage of pure or highly enriched oxygen gas is nowadays ubiquitous in various industrial technologies because of increased efficiency and/or the uniqueness of chemical processes requiring it. Enriched oxygen gas is essential, among others, in the production processes of steel and non-ferrous metals, chemicals, petrochemicals, glass, ceramics, and paper, and also it is utilized in healthcare and medical treatments.[1] At a large scale, the oxygen is produced by cryogenic methods, which involve large capital investment, require specific conditions of pressure and temperature, and consequently, are considered highly energy-consuming and costly.[2] Alternative methods rely on the separation of air components *via* pressure- and/or temperature-driven adsorption processes[3,4] and the emerging membrane-related technologies.[5,6]

Interestingly, with the recent progress in the field of so-called oxygen storage materials (OSMs), several novel compounds appear to be capable of economical production of oxygen by using thermal or pressure swing-type reactions.[7–11] Moreover, depending on their intrinsic properties, these OSMs are also considered for implementation in many important existing and emerging technological processes: for example, inert gas purification; solar water splitting; non-aerobic oxidation including flameless combustion (*e.g.*, synthesis gas production); high-temperature production of steel, glass or plastic production that requires high-purity oxygen; oxy-fuel and chemical looping combustion processes; solid oxide fuel cell technology and the three-way catalytic converters for automotive exhaust systems.[12–21]

[a] *AGH University of Science and Technology, Faculty of Energy and Fuels, Department of Hydrogen Energy, al. A. Mickiewicza 30, 30-059 Krakow, Poland*
[b] *AGH Centre of Energy, AGH University of Science and Technology, ul. Czarnowiejska 36, 30-054 Krakow, Poland*
[c] *Shibaura Institute of Technology, Department of Engineering Science and Mechanics, 3-7-5 Toyosu, Koto-ku, 135-8548 Tokyo, Japan. E-mail: klimkowicz.alicja.ewa.j2@shibaura-it.ac.jp*
[d] *Department of Physics, Northern Illinois University, DeKalb, IL 60115, USA*
[e] *Department of Physics, The Catholic University of Korea (CUK), Bucheon 14662, Korea*

† Electronic supplementary information (ESI) available. See DOI: 10.1039/c7cp03556j

The underlying basis of oxygen incorporation/release into/from OSMs is associated with a large change of the oxygen stoichiometry in the bulk of the material, which is essentially a redox-type process.[10,11,21] For example, as reported by Motohashi *et al.*[10] for the A-site layer-ordered perovskite system, $BaYMn_2O_{5+\delta}$, a reversible change in the oxygen content between O_5 (δ = 0) and O_6 (δ = 1) compositions (3.85 wt% theoretical change) is achievable during an oxygen partial pressure swing process (by reduction in 5 vol% H_2/Ar and oxidation in air) at 500 °C. The reduction time of the powdered $BaYMn_2O_6$ sample was shown to be in the order of minutes at 500 °C, with a practical oxygen storage capacity (OSC) exceeding 3.7 wt%.[11] Oxidation performed in air at the same temperature proceeded much faster (seconds), which was mainly caused by an exothermic reaction ($\sim$200 kJ mol^{-1}) associated with oxygen incorporation.[22] Consequently, it was found that the reduction process is a limiting factor for maximizing the OSC of such compounds.

Partial substitution of selected lanthanides at the Y-site increased reduction rates, for instance, for $BaY_{0.75}Pr_{0.25}Mn_2O_{5+\delta}$ compound, the OSC remained above 3.5 wt%.[23] In another approach, Motohashi *et al.* showed that $BaYMn_2O_6$ powder with an increased specific surface area exhibits faster oxygen release and intake rates.[24] Similar enhancement of the oxygen exchange rates by high-energy mechanical milling was also recently reported for $BaPrMn_2O_{5+\delta}$ and $BaSmMn_2O_{5+\delta}$ materials.[25]

Alternative to materials using the oxygen partial pressure swing process, the hexagonal-type manganites $LnMnO_{3+\delta}$ (Ln = smaller lanthanides, *e.g.* Dy, Ho, Er and Y) were found to operate in the much more promising temperature swing process in pure oxygen or air, as recently documented by Remsen *et al.*[7] and Abughayada *et al.*[8,26] The advantage of such compounds stems from a low and narrow temperature range at which the oxygen exchanges occur, and most importantly, there is no need to use special gas mixtures for the reduction process. However, the kinetics of the redox processes reported to date have been relatively slow, and the achievable OSC has been somewhat lower than that for the layer-ordered perovskites.[9,23] The substitutions and processing related improvements of redox properties observed for layered perovskites suggest that similar improvements should be possible for hexagonal manganites.

The $LnMnO_{3\pm\delta}$ manganites are known to exhibit the perovskite- or hexagonal-type crystal structure depending on the size of the lanthanide and, to some degree, on the oxygen content during the synthesis.[26,27] For larger lanthanides (La–Dy), the distorted perovskite structure is observed when synthesized in air. For smaller ones (Ho–Lu, In and Sc), the hexagonal structure (Hex0, δ = 0) is formed with layers of 8-fold coordinated Ln^{3+} cations and layers of the corner-shared MnO_5 trigonal-bipyramids.[8,26] This five-fold coordination of Mn^{3+} causes splitting of the $3d^4$ electronic orbitals into three sets: empty a′ (d_{z^2}) and filled up e′ ($d_{x^2-y^2}$, d_{xy}) and e″ (d_{xz}, d_{yz}) with high spin states e'^2 and e''^2. As a result of orbital filling, the elongation of basal Mn–O bonds and the compression of the apical Mn–O bond are observed. Interestingly, it was shown that the stable hexagonal phase can be converted to the perovskite one by special treatments, *e.g.*, high pressure,[28,29] deposition of strained thin films[30] or by using soft chemistry methods, followed by appropriate annealing.[31] The reverse conversion of the perovskite to the hexagonal structure under reducing conditions was also documented for $DyMnO_3$.[7]

Until the recent reports by Remsen *et al.* regarding $DyMnO_{3+\delta}$ and substituted $Dy_{1-x}Y_xMnO_{3+\delta}$,[7,31] not much was known about the oxygen hyperstoichiometry in hexagonal manganites. The subsequent paper focused on the structural, magnetic and oxygen storage-related properties of the $Dy_{1-x}Y_xMnO_{3+\delta}$ series,[26] in which the superstructure *R3c* (tripled along the *c*-axis, Hex1) of $Dy_{0.7}Y_{0.3}MnO_{3.29}$ was reported. Furthermore, similar behavior was also observed for the hexagonal $HoMnO_{3+\delta}$, $ErMnO_{3+\delta}$, and $YMnO_{3+\delta}$, obtained by high oxygen pressure annealing (Hex2, $\delta \approx 0.41$) for which OSC, as well as the temperatures of oxidation and reduction, were reported depending on the ionic radius of R^{3+}.[8] However, because the observed kinetics of the oxidation/reduction processes were very slow, the determination of the respective phase diagrams of stability of the stoichiometric and oxygen-loaded phases was not complete. Moreover, such a slow kinetics was responsible for the reduced OSC, which could hinder applicability of hexagonal $LnMnO_{3+\delta}$ manganites for use at elevated temperatures where waste heat is frequently available from several industrial processes.

In this work, we report on the structural and oxygen content changes of the selected $HoMnO_{3+\delta}$ materials at the stability boundary in air of the hexagonal phase recorded during long-time *in situ* oxidation and reduction at elevated temperatures and in constant oxygen partial pressure conditions of pure oxygen and air. Despite a very small difference in the ionic sizes of Ho and $Dy_{1-x}Y_xMnO_{3+\delta}$, a significant difference in redox reactions is observed. Synthesis and processing methods have a large effect on the properties as well. A discussion pertaining to the size of substituted Ln cation and the sample preparation method is given on the oxygen storage-related properties, such as the temperature and speed of the oxygen intake and release, the oxygen storage capacity, and the phase stability of the materials. It is shown that enhancement of the OSC characteristics can be achieved by high-impact ball-milling, which produces powders with an increased specific surface area. The valence states of Mn and Ho ions in $HoMnO_{3+\delta}$ were determined by employing soft X-ray absorption spectroscopy (XAS), where synchrotron radiation is used as the excitation photon source. XAS is known to be a powerful experimental tool for studying the electronic structures of solids,[32,33] such as the valence and spin states of the constituent transition-metal and rare-earth ions.

2. Experimental procedures

2.1 Material preparation

The reference Hex0 hexagonal $HoMnO_3$ 0MM (non-milled) samples for *in situ* X-ray and thermogravimetric measurements were synthesized by a typical high-temperature ceramic method from MnO_2 and Ho_2O_3 oxides. Stoichiometric proportions of the oxides were mechanically milled under dry conditions using zirconia balls to powder at a ratio of 8 : 1, pressed into

pellets and, to obtain small grain samples, sintered at a low temperature of 1050 °C for 8 h in air followed by fast cooling to room temperature (RT). A part of the sample, denoted as 15MM, was additionally subjected to high-energy milling, conducted using a Fritsch planetary ball mill, model P7, for 15 minutes, with a rotational speed of 400 rpm. An additional set of large-sized grains of $HoMnO_3$ 0MM samples using X-ray absorption spectroscopy and magnetic measurements was obtained with the precisely defined oxygen contents by utilizing information obtained from the *in situ* X-ray and thermogravimetric measurements, 3.00 (Hex0, as synthesized in air at 1400 °C followed by fast cooling to RT), 3.39 (Hex2, obtained by high-pressure oxygen annealing under 215 bar of pure oxygen at 400 °C followed by slow cooling of the as-made sample to RT) and 3.28 (Hex1, obtained by annealing in oxygen at 270 °C followed by fast cooling to RT of the high pressure oxygen loaded sample).

2.2 Material characterization

The structural X-ray studies of the synthesized oxides were carried out at room temperature (RT) in the range of 10–110 degrees with CuK_α radiation using a PANalytical Empyrean diffractometer. For high-temperature measurements, an Anton Paar HTK 1200N oven-chamber was installed. Measurements in pure O_2 using a flow rate of 100 cm^3 min^{-1} were conducted for 15 min per scan. To observe the structural changes during the long-term oxidation at a carefully chosen temperature, the sample was rapidly heated (*ca.* 5 min) to 250 °C. Additional measurements were conducted for the temperature increases and decreases of 10 °C in a range of 220–300 °C for the $HoMnO_{3+\delta}$ 15MM sample. The XRD tests of the phase stability and thermal expansion in air were also carried out up to 900 °C with the data taken every 100 °C. The GSAS/EXPGUI set of software was used for the Rietveld analysis of the data.[34,35]

Scanning electron microscopy (SEM) evaluation of the chemical composition and the element mapping were done for powders using JEOL JSM-7610F apparatus equipped with an EDS detector by using a magnification range of 1000–10 000.

The OSCs during reduction/oxidation runs were determined by using the thermogravimetric (TG) method. All experiments were conducted on a TA Q5000 IR apparatus. For all the studies, either pure O_2 or synthetic air flow at 100 cm^3 min^{-1} and heating rates of 0.1–5° min^{-1} were used. Prior to the studies in an oxygen atmosphere, all the investigated samples were heated up to 500 °C and cooled down to RT with a heating rate of 5° min^{-1} in a flow of synthetic air to remove possible surface contamination. As shown in the following paragraphs, this annealing resulted in a slight oxygen adsorption and $\delta > 0$ for some of the samples at the beginning of the TG experiments. The temperatures of reduction and oxidation, T_{red} and T_{oxi}, were evaluated by determining the extremes of the derivative of the TG curve. Stability studies were also conducted in air atmosphere for 7 days at the temperatures where maximum oxygen content was observed as determined from the TG measurements. Based on previous reports,[7,8] the oxygen content was fixed as equal to 3 ($\delta = 0$) at 500 °C.

XAS measurements were performed at the 2A undulator beamline of PLS-II (Pohang Light Source-II) by employing the total electron yield (TEY) method. Samples were cleaned *in situ* in vacuum by repeated scraping with a diamond file under pressure higher than 2×10^{-10} Torr. XAS data were obtained at $T \sim 350$ K in order to reduce the charging problem in these insulating oxides. The experimental energy resolution for the XAS data was set to ~100 meV at $h\nu \sim 600$ eV. All the XAS spectra were normalized to the incident photon flux. Magnetization measurements were performed using a Magnetic Property Measurement System (Quantum Design). Temperature dependence of magnetization was measured in a magnetic field $H = 1$ kOe in the temperature range of 2–395 K, initially in a "zero field cooling" mode (cooling the sample to $T = 2$ K in a zero magnetic field, switching a magnetic field on, and measuring upon warming), then in a "field cooling" mode (measuring upon cooling in a magnetic field) and finally the remanent magnetization was measured upon warming in the zero magnetic field after switching the magnetic field off at $T = 2$ K.

3. Results and discussion

3.1 Structure and the oxygen storage properties of $HoMnO_{3+\delta}$ during temperature swing in oxygen

To observe the structural evolution caused by oxygen incorporation *in situ*, the oxygen stoichiometric, nearly single-phase $HoMnO_3$ 15MM (containing traces of Ho_2O_3) sample was rapidly, in about 5 min, heated from room temperature to 250 °C and held in pure oxygen for 20 hours. As can be seen from the time-dependent XRD data presented in Fig. 1a, the $HoMnO_3$ 15MM transforms completely from Hex0, the $P6_3cm$ ($\delta \approx 0$) phase to the oxidized phase Hex1, $R3c$ ($\delta \approx 0.28$) in a matter of 8–10 hours. The progression of structural transition is relatively slow, and therefore, easily observable during XRD measurements when the $P6_3cm$ (Hex0) diffraction peaks gradually disappear and the $R3c$ peaks (Hex1) emerge. During oxidation, oxygen is intercalated into the Mn–O sublattice, resulting in an increase in the average Mn coordination number from 5 in trigonal-bipyramids to an average of 8, while the 8-fold Ln–O coordination is preserved. However, some of the allowed 8 oxygen sites around the Mn ion are only partially occupied to satisfy the proper bond lengths. A fraction of the oxygen ions becomes shifted from their original positions, which together with the incorporation of additional oxygen results in a rearrangement of the stacking mode of the Mn–O layers, and the formation of the $R3c$ superstructure with a tripling of the *z*-parameter along the *c*-axis, as documented in previous works.[8,26] In particular, no peak shift is observed during the oxidation process, which confirms that the mechanism of the transition is a two phase-like, *i.e.*, there are no regions in the material having an intermediate oxygen content.

Refinement of the data presented in Fig. 1a allowed for the determination of changes in the phase content in the studied material, with disappearance of the Hex0 phase and formation of the Hex1 phase as presented in Fig. 1b (circles). The nature of this transition (rate-controlling process) was examined by

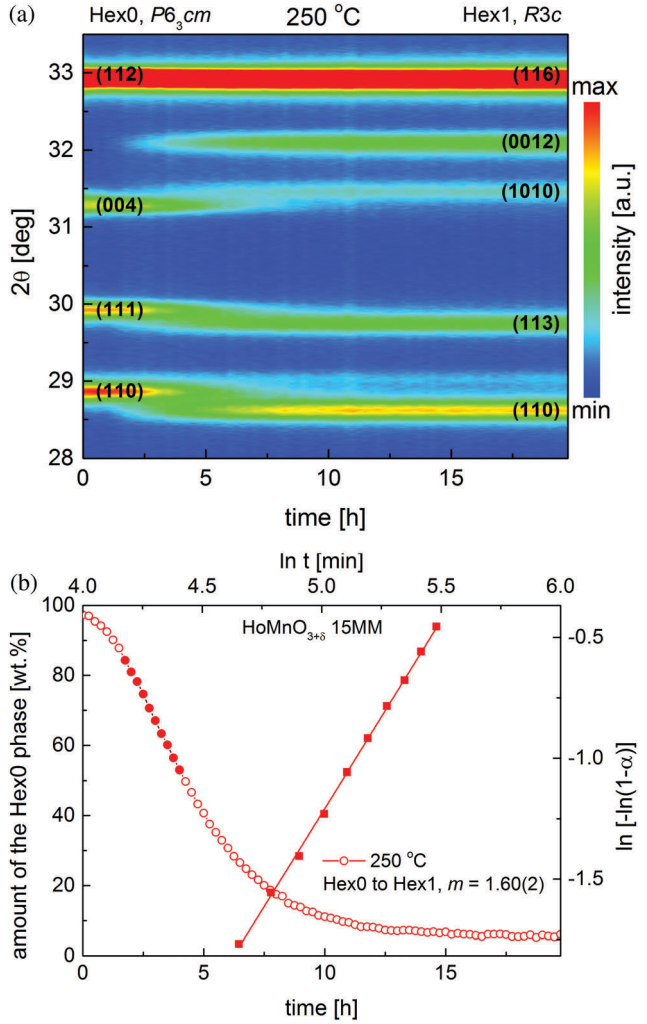

Fig. 1 (a) Isothermal *in situ* XRD matrix showing the oxidation of $HoMnO_3$ 15MM in an oxygen atmosphere from Hex0 ($P6_3cm$) to Hex1 ($R3c$) at 250 °C, visible as intensity change of the reflections, and (b) time dependence of the refined weight ratio of the reduced Hex0 phase together with the $\ln(-\ln(1-\alpha))$ *vs.* $\ln(t)$ plot.

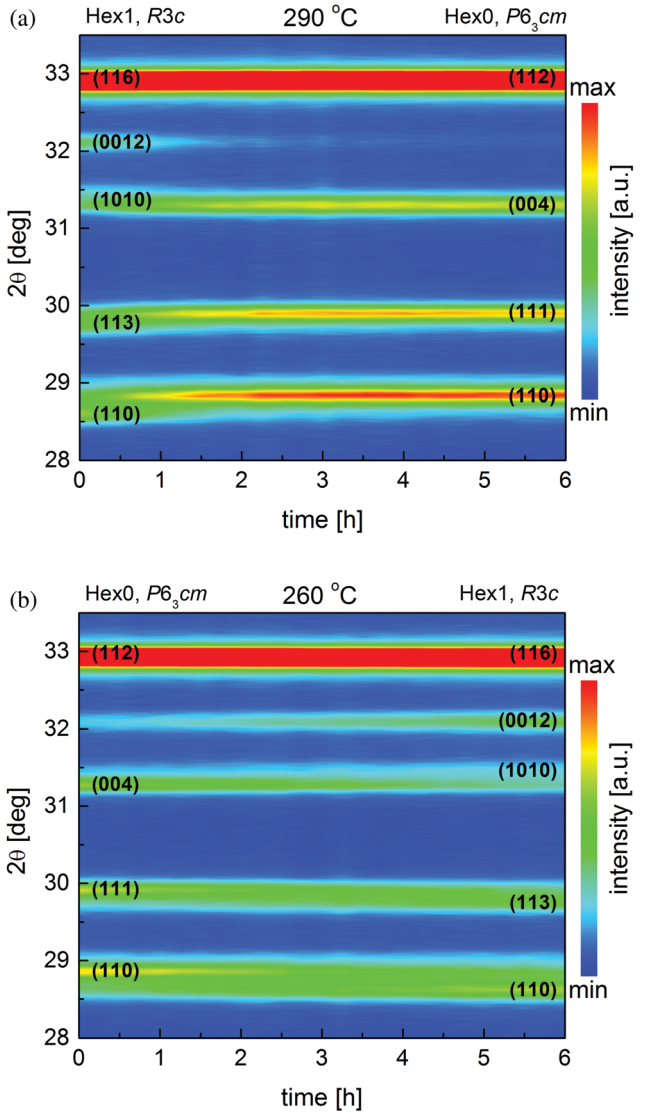

Fig. 2 Isothermal *in situ* XRD matrix showing (a) complete reduction of $HoMnO_{3+\delta}$ 15MM from Hex1 ($R3c$) to Hex0 ($P63cm$) at 290 °C, and (b) reoxidation of $HoMnO_3$ 15MM from Hex0 to Hex1 at 260 °C in the oxygen atmosphere, visible as intensity change of the reflections.

using the approach presented by Motohashi *et al.*[36] for the determination of the properties of the $BaYMn_2O_{5+\delta}$ system. Following the Avrami equation, a plot of $\ln(-\ln(1-\alpha))$ *vs.* $\ln(t)$ has been obtained, in which α is a time-dependent fraction of the reacted phase *i.e.*, Hex0 (squares in Fig. 1b). The typical range of data, $0.15 < \alpha < 0.5$ (corresponding to the full circles), was used in calculations,[37] as presented in Fig. 1b. The fitted value of the slope coefficient m was found to be equal to 1.6, suggesting, according to the Hancock and Sharp approach, a large influence on the surface reaction and new phase nucleation, both limiting the speed of the oxidation process.[36,37]

Additional detailed structural evaluation of the oxidized $HoMnO_{3+\delta}$ 15MM sample was done in the temperature range of 220–300 °C. Starting from the fully oxidized Hex1 material at 250 °C, the temperature was increased by 10 °C each time, and then 24 consecutive isothermal scans, each lasting ~15 min, were carried out for a total of 6 hours. No changes in the crystal structure of the Hex1 material, besides the thermal lattice expansion, were observed up to 270 °C. At 280 °C, the stoichiometric Hex0 phase begins to form, however, due to very slow kinetics at that temperature, the transition did not proceed to completion after 6 hours. Nevertheless, at 290 °C, a complete disappearance of the Hex1 peaks and emergence of the Hex0 peaks could be clearly observed (Fig. 2a). At 300 °C, the sample retained the Hex0 structure. The results presented here show that the phase stability diagram (in oxygen) of the various $LnMnO_{3+\delta}$ oxides, as obtained by Abughayada *et al.*,[8] during a faster heating procedure is not precise. In this particular case of $HoMnO_{3+\delta}$ 15MM, the estimated temperature of the Hex1 → Hex0 phase transition on heating by long-time equilibration experiments is about 40 °C lower than that reported in ref. 8. This discrepancy can be explained by taking into account the

influence of mechanical milling that lowers the particle size and breaks the agglomerates, on the properties of the material. As shown before for $BaLnMnO_{5+\delta}$ Ln = Pr, Sm, milling significantly lowers the characteristic temperature of reduction.[25] In addition, since the oxygen partial pressure (pO_2) was kept constant during experiments (1 atm), from the thermodynamic point of view, there should be no regions in the equilibrium phase diagram with both phases thermodynamically stable. However, due to the limitations of slow kinetics (the new phase nucleation and growth, *etc.*), such mixed-phase regions are observed depending on the heating rate or holding time; for example, in the reported case here at 280 °C on heating, the equilibrium is not achieved during the 6 hour hold. However, it could be expected that at this temperature, the Hex0 phase would be stable after a very long equilibration time.

Structural studies of the Hex0 $HoMnO_3$ 15MM sample continued during the cooling down experiments from 300 °C to 220 °C. At 270 °C, traces of the oxidized Hex1 phase were already detected; however, during 6 hour time of the measurements, the transition was not finished. A decrease in temperature down to 260 °C caused further structural transformation of the material (Fig. 2b); however, the Hex0 phase completely disappeared only at 240 °C. This is in agreement with our initial observation of the Hex0 phase transformation to Hex1 at 250 °C, which took about 8–10 hours, so it was not completed here upon cooling at 250 °C during the 6 hour hold. The single-phase Hex1 was preserved down to 220 °C and no traces of the more oxidized Hex2 phase were detected. Considering very slow kinetics and the appearance of the Hex1 phase already at 270 °C upon cooling, the temperature hysteresis of the Hex0 ↔ Hex1 transition could possibly be estimated as only 10 °C (280 °C upon heating, 270 °C upon cooling). A small value of the hysteresis temperature of transitions is an important parameter for conceivable application of OSM utilizing temperature swing processes.[8]

Calculated unit cell volumes V of the Hex0 and Hex1 phases during heating (250–300 °C) and cooling (300–220 °C), and during additional heating (220–250 °C) are presented in Fig. 3 (unit cell parameters a and c are shown in Fig. S1a and b, ESI†). The c and V parameters were normalized for the $R3c$ phase by dividing by 3. Interestingly, for the newly appearing phases (*i.e.* Hex0 at 280 °C upon heating and Hex1 at 270 °C upon cooling), the calculated parameters diverge from the overall trend, which can be associated with the internal strain, evolution of the oxygen content in forming phases or resulting from the two-phase refinement of poorly formed phases. Deviation from the general trend is much more visible for the parameter a, because the additional oxygen is preferentially incorporated into or removed from the Mn–O planes. The final XRD data created by adding up all the 24 measurements at respective temperatures for the single-phase phases Hex0 at 300 °C and Hex1 at 220 °C are presented in Fig. 4, together with the Rietveld refinements using the $P6_3cm$ and $R3c$ space groups, respectively. The structural parameters are listed in Table 1.

Changes in the oxygen stoichiometry with temperature for the $HoMnO_{3+\delta}$ 15MM sample were investigated using the thermogravimetric technique and compared with the structural data.

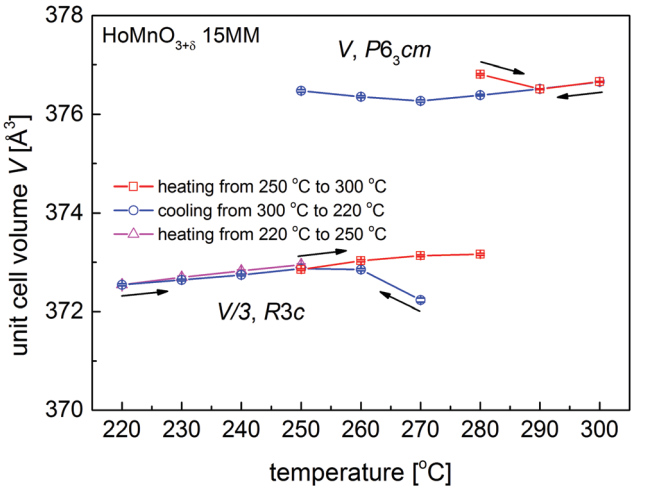

Fig. 3 Evolution of the unit cell volume of $HoMnO_{3+\delta}$ 15MM upon heating and cooling in an oxygen atmosphere. A sequence of the measurement and the range of existence of Hex0 ($P6_3cm$) and Hex1 ($R3c$) phases is shown.

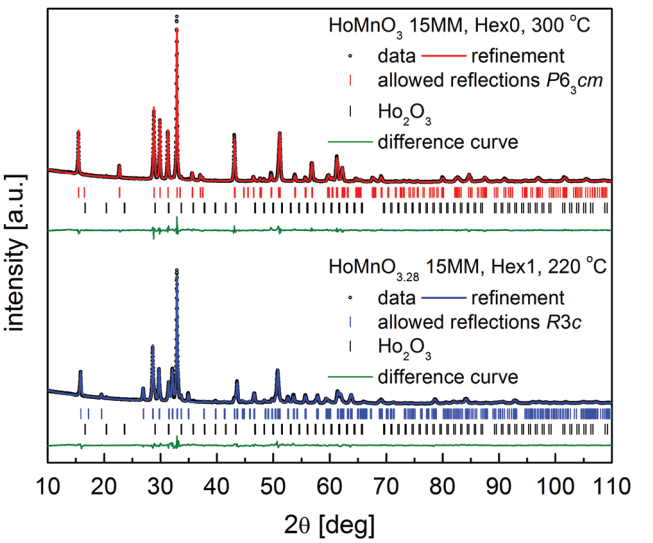

Fig. 4 Diffractograms with Rietveld analysis for: $HoMnO_3$ 15MM at 300 °C (Hex0), and $HoMnO_{3.28}$ 15MM at 220 °C (Hex1); see details in the text.

Table 1 Structural parameters of $HoMnO_{3+\delta}$ 15MM at high temperatures

Phase composition	T [°C]	Space group	a [Å]	c [Å]	V [Å^3]	R_{wp} [%]
Hex0, $\delta = 0$	300	$P6_3cm$	6.1769(1)	11.3993(2)	376.66(1)	2.27
Hex1, $\delta = 0.28$	220	$R3c$	6.2181(1)	33.3777(9)	1117.63(6)	2.32

The results of the temperature swing processes carried out consecutively at different heating rates (5° min^{-1}, 1° min^{-1}, and then 0.1° min^{-1}) are presented in Fig. 5a. For comparison, the data for the initial $HoMnO_{3+\delta}$ 0MM sample are shown in Fig. 5b. Based on these measurements, the oxygen storage-related properties of the studied samples have been derived and are presented in Table 2. While comparing the oxygen

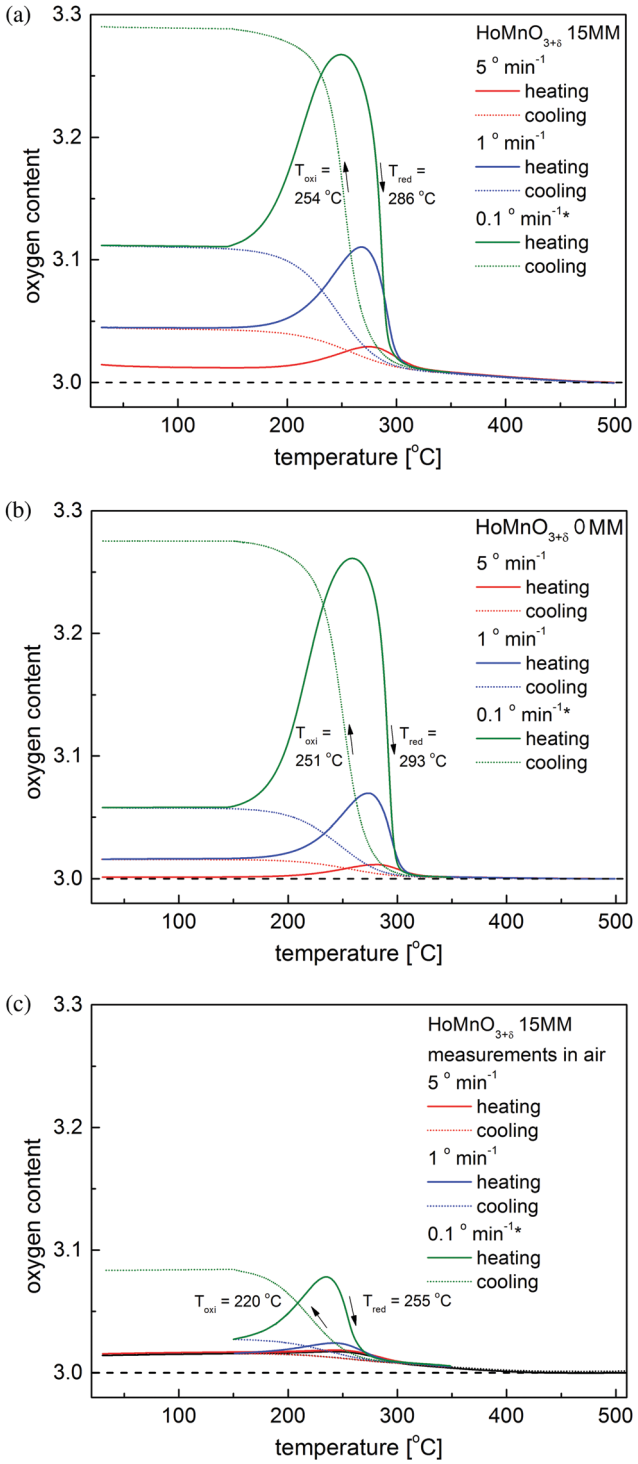

Fig. 5 Temperature dependence of the oxygen content registered during heating and cooling with various rates for (a) $HoMnO_{3+\delta}$ 15MM, (b) for $HoMnO_{3+\delta}$ 0MM in an O_2 atmosphere, and (c) $HoMnO_{3+\delta}$ 15MM in air. *Below 150 °C, the heating/cooling rate was 1° min^{-1}.

incorporation into the as-obtained material and the ball-milled sample, some increase in the speed of the processes can be observed as a higher oxygen content at the respective maxima for the same heating/cooling speeds and a small decrease in the temperature hysteresis of the Hex0 ↔ Hex1 transition $\Delta T = T_{red} - T_{oxi}$ can be observed for the 15MM sample. This is consistent with the SEM results (Fig. S2 and S3, ESI†), showing no significant effect of mechanical milling process on the morphology of the powders. Furthermore, EDX elemental mapping showed the expected, homogeneous distribution of the elements in the initial, as well as in the milled samples.

3.2 Occurrence of the oxidized $HoMnO_{3.28}$ 15MM Hex1 phase in air

As shown above, the temperature swing process progresses effectively for $HoMnO_{3+\delta}$ 0MM and $HoMnO_{3+\delta}$ 15MM in an atmosphere of pure oxygen. It was therefore of interest to investigate if the oxidized Hex1 phase would also appear in air at elevated temperatures. Initial high-temperature XRD measurements have shown no presence of the Hex1 phase for the $HoMnO_3$ 15MM sample in air up to 900 °C. Since the oxygen stoichiometry was preserved, these measurements allowed for the calculation of the Hex0 unit cell parameters and the determination of the thermal expansion coefficient (TEC), as depicted in Fig. 6. The thermal expansion was found to be highly anisotropic, with almost no change in the c parameter up to 400 °C and a slight decrease at higher temperatures indicating persistence of filling the e'^2 and e''^2 electronic orbitals of MnO_5. The unit cell volume-based values were refined as $TEC_{25-500°C} = 10.7(3) \times 10^{-6}\ K^{-1}$ and $TEC_{500-900°C} = 12.8(1) \times 10^{-6}\ K^{-1}$ for the Hex0 phase, which are comparable with Dy-rich $Dy_{1-x}Y_xMnO_3$.[7]

Additionally, more accurate diffraction measurements were performed every 10 °C in the 200–300 °C temperature range (Fig. S4, ESI†), clearly indicating an appearance of a low-intensity extra reflection at 220–260 °C, which was identified as the (0012) diffraction peak of the oxidized Hex1 phase. By considering the slow kinetics of the Hex0 ↔ Hex1 transitions observed in the oxygen (Fig. 5a and b), the additional long-term, 7 day annealing tests were conducted for the $HoMnO_{3+\delta}$ 15MM sample in air at 250 °C. As shown in Fig. 7, the Rietveld analysis indicated the two-phase mixture of about 70 wt% of the oxidized Hex1 and 30 wt% of Hex0 phases, which would indicate the total oxygen content of about 3.20. Thermogravimetric measurements (Fig. 5c) confirmed the partial oxidation of the material in air; however, the amount of incorporated oxygen, even during slow cooling (0.1° min^{-1}), was relatively small, $\delta \approx 0.08$. Remarkably, the Hex1 to Hex0 transition temperature upon heating $T_{red} \approx 255$ °C was found to be significantly lower than that in the oxygen, *ca.* 290 °C, implying its strong dependence on the oxygen pressure. The excess oxygen achieved in air during a TG experiment is lower than that observed for $DyMnO_{3+\delta}$ ($\delta \approx 0.22$) (see Fig. 3 in ref. 7), but confirms the temperature swing process conducted in air to be successful for smaller size lanthanide hexagonal manganite $HoMnO_{3+\delta}$ that can be easily prepared in air. It seems thus that the proper selection of lanthanide could open a possibility for the usage of hexagonal manganites as OSMs in air at controllable temperatures in the range of 200–300 °C, where the waste heat is frequently available in many industrial processes.

Table 2 Oxygen storage-related properties of the studied oxides

Chemical composition	Atmosphere	OSC between RT and 500 °C [wt%]	Maximum oxygen content during 0.1° min^{-1} heating	Temperature of the maximum oxygen content on 0.1° min^{-1} heating [°C]	ΔT [°C]
$HoMnO_{3+\delta}$ 0MM	Oxygen	1.64	3.26	260	42
$HoMnO_{3+\delta}$ 15MM	Oxygen	1.73	3.27	250	32
$HoMnO_{3+\delta}$ 15MM	Air	0.50	3.08	235	35

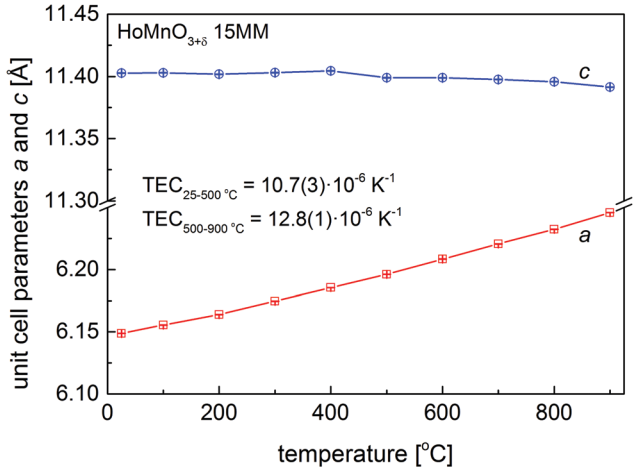

Fig. 6 Temperature dependence of the unit cell parameters a and c for $HoMnO_{3+\delta}$ 15MM, recorded during heating up to 900 °C in an air atmosphere, together with the calculated thermal expansion coefficients.

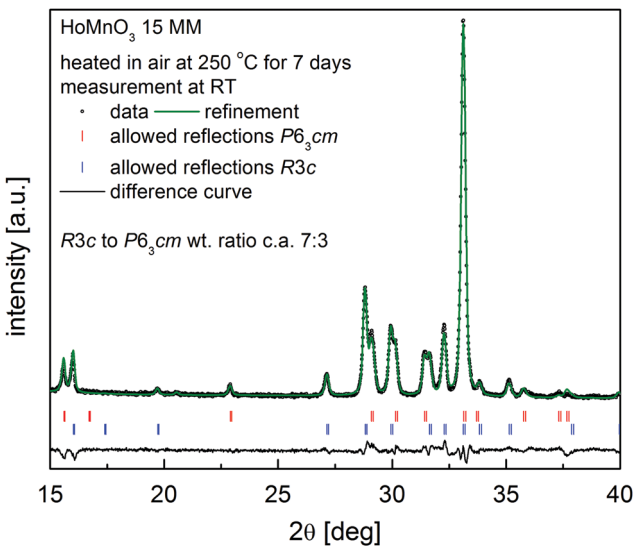

Fig. 7 XRD pattern together with Rietveld analysis for the $HoMnO_{3+\delta}$ 15MM sample after heating at 250 °C in air for 7 days, showing the formation of ~70 wt% of the oxidized Hex1 phase.

3.3 Valence states of Mn and Ho ions in $HoMnO_{3+\delta}$ 0MM determined from XAS

Fig. 8a shows the Mn 2p (L-edge) XAS spectra of $HoMnO_{3+\delta}$ 0MM (δ = 0, 0.28, 0.4), measured at T = 350 K. As a guide to the valence states of Mn ions in $HoMnO_{3+\delta}$ 0MM, they are compared with those of reference Mn oxides of formally divalent (Mn^{2+}) MnO, formally trivalent (Mn^{3+}) Mn_2O_3, and formally tetravalent (Mn^{4+}) MnO_2.[38,39] L_3 ($2p_{3/2}$) and L_2 ($2p_{1/2}$) peaks arise from the spin–orbit splitting of the Mn 2p core levels. The weakly negative slope for the δ = 0 sample (Hex0) is due to charging in the Hex0 sample. It is well known that the Mn 2p XAS peak positions shift toward higher energies as the Mn valence increases.[36,38] This figure shows clearly that the peak positions of the Mn 2p XAS spectra of $HoMnO_{3+\delta}$ 0MM shift as δ changes, with the accompanying changes in their line shapes. The Mn 2p XAS spectrum of δ = 0 (Hex0) is very similar to that of Mn_2O_3, while that of δ = 0.4 (Hex2) is similar to that of MnO_2 and that of δ = 0.28 (Hex1) is in between those two. These differences provide evidence that the valence states of Mn ions, ν(Mn), increase monotonically from δ = 0 to δ = 0.4. In other words, ν(Mn) ≈ 3+ at δ = 0 to ν(Mn) ≈ 4+ at δ = 0.4. These Mn 2p XAS results support the oxygen content determined by the TG method (see Fig. 5 and Table 2).

In contrast, as shown in Fig. 8b, the Ho 3d (L-edge) XAS spectra of $HoMnO_{3+\delta}$ 0MM (δ = 0, 0.28, 0.4) do not change for the varying δ. This observation indicates that the valence states of Ho ions do not change with δ, keeping the trivalent states (Ho^{3+}) for all δ. Our XAS study for Mn 2p and Ho 3d states suggests that the excess oxygen in $HoMnO_{3+\delta}$ 0MM causes the electron transfer from Mn^{3+} to O (oxygen), resulting in Mn^{4+} at δ = 0.4 (Hex2) and Mn^{3+}–Mn^{4+} mixed-valent at δ = 0.28 (Hex1), but the excess oxygen does not affect Ho ions in $HoMnO_{3+\delta}$ 0MM.

3.4 Magnetic measurements of oxygen loaded $HoMnO_{3+\delta}$ 0MM

Temperature dependences of the molar magnetic susceptibility for $HoMnO_{3.28}$ 0MM and $HoMnO_{3.39}$ 0MM are presented in Fig. 9. A cusp in the "zero field cooled" magnetization is observed at T = 6.5 K for both compositions. The "zero field cooled" and "field cooled" magnetizations show irreversibility at low temperatures. The above features together with an observation of the remanent magnetization point at possible spin glass behavior in both materials. The inverse molar susceptibility presented in the insets for the "field cooled" measurements demonstrate a linear behavior above T ~ 150 K. We fitted our susceptibility data to a modified Curie–Weiss formula $\chi = \chi_0 + (1/8) \times \mu_{eff}^2 \times (T - T_C)$, where χ is the molar susceptibility, χ_0 is the background susceptibility, $\mu_{eff} = gS(S+1)$ is the paramagnetic effective moment, S is the magnetic spin, and g = 2 is the Lande factor. The fitting results for the "field cooled" data in the temperature range of 200–390 K give the values of μ_{eff} approximately equal to 9.2 μ_B (Bohr magnetons) and 9.25 μ_B for $HoMnO_{3.28}$ 0MM and $HoMnO_{3.39}$ 0MM, respectively. The susceptibility is dominated by the magnetic contribution of Ho^{3+} moments (μ_{eff}^{Ho} = 10.6 μ_B). An addition of

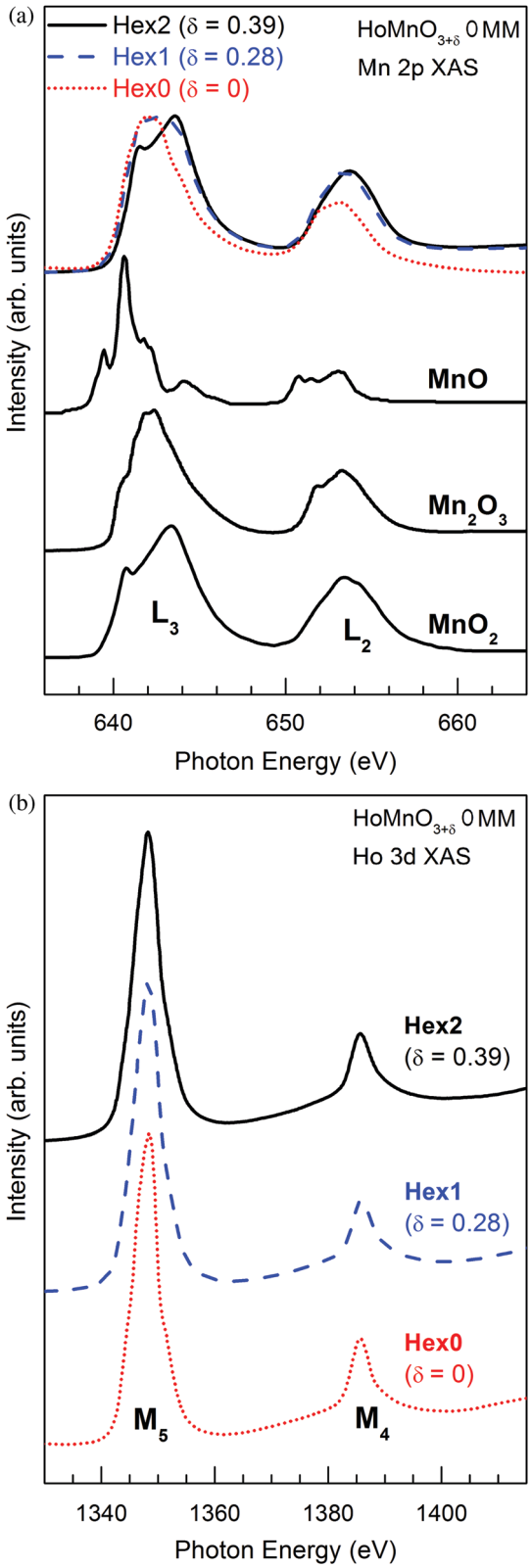

Fig. 8 XAS spectra of $HoMnO_{3+\delta}$ 0MM (δ = 0, 0.28, 0.4) measured at T = 350 K for (a) the Mn 2p (L-edge) and (b) the Ho 3d (L-edge).

Mn^{3+} (μ_{eff}^{Mn} = 4.9 μ_B) or Mn^{4+} (μ_{eff}^{Mn} = 3.87 μ_B) both present in $HoMnO_{3+\delta}$ 0MM materials would give the total effective moment

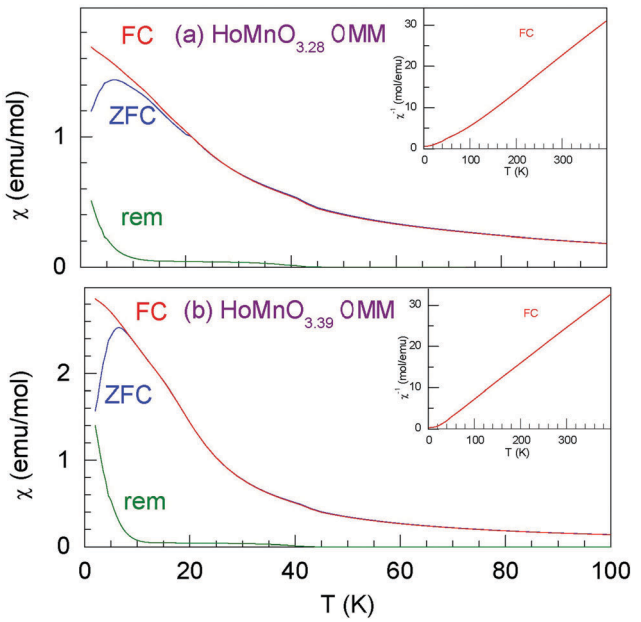

Fig. 9 Temperature dependence of molar magnetic susceptibility for (a) $HoMnO_{3.28}$ 0MM and (b) $HoMnO_{3.39}$ 0MM, determined from magnetization measured in a magnetic field H = 1 kOe in "zero field cooled" (ZFC), "field cooled" (FC), and "remanent" (rem) modes (see text). Insets show temperature dependences of inverse magnetic susceptibility.

according to the simple formula $(\mu_{eff})^2 = (\mu_{eff}^{Ho})^2 + (\mu_{eff}^{Mn})^2$, which gives μ_{eff} = 11.68 μ_B for Mn^{3+} and μ_{eff} = 11.28 μ_B for Mn^{4+} that are close to each other, and a small change in the Mn valence results in a hardly detectable change in μ_{eff}. Our values of μ_{eff} are significantly smaller than those expected from the above-simplified model. The same discrepancy was observed for $Dy_{1-x}Y_xMnO_{3+\delta}$ materials.[26]

4. Conclusions

Hexagonal $HoMnO_{3+\delta}$ manganites prepared by various methods exhibit interesting properties related to their application in the thermal swing process of oxygen incorporation and release. The long-term annealing experiments have shown that a Hex0 → Hex1 transition for $HoMnO_{3+\delta}$ 15MM is limited by the surface reaction and nucleation of the new phase. The temperatures of reversible Hex0 ↔ Hex1 structural transitions caused by a change in oxygen stoichiometry between δ = 0 and 0.28 have been established as 290 °C on heating and 250 °C on cooling, also indicating that temperature hysteresis of the transition could possibly be as small as 10 °C. High impact ball-milling for 15 min had only a small effect on improving the speed of the reduction/oxidation processes. Interestingly, the Hex1 phase for the $HoMnO_{3+\delta}$ 15MM material can also be obtained by prolonged heating in air at a temperature range of 220–255 °C, which is important for practical applications of the thermal swing process.

X-ray absorption spectroscopy measurements confirmed that oxygen loading of the $HoMnO_{3+\delta}$ 0MM material causes the electron transfer from Mn^{3+} to oxygen, resulting in Mn^{4+} at

δ = 0.39 (Hex2) and Mn^{3+}–Mn^{4+} mixed-valent at δ = 0.28 (Hex1), but that the excess oxygen does not affect Ho ions in $HoMnO_{3+\delta}$ 0MM. An attempt to resolve the effective Mn valence from magnetic susceptibility data gave inconclusive results due to dominating magnetism of Ho^{3+} ions.

Comparison of hexagonal $HoMnO_{3+\delta}$ with $DyMnO_{3+\delta}$ and substituted $Dy_{1-x}Y_xMnO_{3+\delta}$ materials indicates that a tiny increase in the ionic size of the lanthanide has a huge effect on the redox properties of hexagonal manganites. As such, an increased effort should be directed at synthesizing and studying the larger average size (Y,Ln)$MnO_{3+\delta}$ compounds.

Acknowledgements

This project was funded by the National Science Centre, Poland, on the basis of the decision number UMO-2015/19/B/ST8/00871. The work at the CUK was supported by the Korean National Research Foundation (NRF) under the contract number (No. 2016R1D1A1B03932391). A synchrotron radiation spectroscopy experiment was supported by the PAL (Pohang Accelerator Laboratory) and MSIP in Korea.

References

1 J. Emsley, *Nature's Building Blocks: An A–Z Guide to the Elements*, Oxford University Press, 2001.
2 M. Kanoglu, I. Dincer and M. A. Rosen, *Int. J. Energy Res.*, 2008, **32**, 35–43.
3 D. R. Vinson, *Comput. Chem. Eng.*, 2006, **30**, 1436–1446.
4 Y.-S. Lin, D. Mac Lean and Y. Zeng, *High temperature adsorption process*, *US Pat.*, 6059858, 2000.
5 M. Ulbricht, *Polymer*, 2006, **47**, 2217–2262.
6 S. S. Hashim, A. R. Mohamed and S. Bhatia, *Renewable Sustainable Energy Rev.*, 2011, **15**, 1284–1293.
7 S. Remsen and B. Dabrowski, *Chem. Mater.*, 2011, **23**, 3818–3827.
8 C. Abughayada, B. Dabrowski, S. Kolesnik, D. E. Brown and O. Chmaissem, *Chem. Mater.*, 2015, **27**(18), 6259–6267.
9 A. Klimkowicz, K. Świerczek, A. Takasaki, J. Molenda and B. Dabrowski, *Mater. Res. Bull.*, 2015, **65**, 116–122.
10 T. Motohashi, T. Ueda, Y. Masubuchi, M. Takiguchi, T. Setoyama, K. Oshima and S. Kikkawa, *Chem. Mater.*, 2010, **22**, 3192–3196.
11 K. Świerczek, A. Klimkowicz, K. Zheng and B. Dabrowski, *J. Solid State Chem.*, 2013, **203**, 68–73.
12 T. Kodama and N. Gokon, *Chem. Rev.*, 2007, **107**, 4048–4077.
13 J. Kašpar and P. Fornasiero, *J. Solid State Chem.*, 2003, **171**, 19–29.
14 Z. Yang, Y. S. Lin and Y. Zeng, *Ind. Eng. Chem. Res.*, 2002, **41**, 2775–2784.
15 Y. Wei, H. Wang, F. He, X. Ao and C. Zhang, *J. Nat. Gas Chem.*, 2007, **16**, 6–11.
16 K. Li, H. Wang and Y. Wei, *J. Chem.*, 2013, 294817.
17 K. Wang, Q. Yu and Q. Qin, *J. Therm. Anal. Calorim.*, 2013, **112**, 747–753.
18 S. Bhavsas and G. Veser, *RSC Adv.*, 2014, **4**, 47254–47267.
19 O. L. Pineda, Z. L. Moreno, P. Roussel, K. Świerczek and G. H. Gauthier, *Solid State Ionics*, 2016, **288**, 61–67.
20 J. Vieten, B. Bulfin, F. Call, M. Lange, M. Schmücker, A. Francke, M. Roeba and C. Sattler, *J. Mater. Chem. A*, 2016, **4**, 13652–13659.
21 T. Motohashi, M. Kimura, Y. Masubuchi, S. Kikkawa, J. George and R. Dronskowski, *Chem. Mater.*, 2016, **28**(12), 4409–4414.
22 M. Gilleßen, M. Lumeij, J. George, R. Stoffel, T. Motohashi, S. Kikkawa and R. Dronskowski, *Chem. Mater.*, 2012, **24**, 1910–1916.
23 A. Klimkowicz, K. Świerczek, K. Zheng, M. Baranowska, A. Takasaki and B. Dabrowski, *Solid State Ionics*, 2014, **262**, 659–663.
24 T. Motohashi, T. Ueda, Y. Masubuchi and S. Kikkawa, *J. Ceram. Soc. Jpn.*, 2011, **119**, 894–897.
25 A. Klimkowicz, K. Świerczek, T. Yamazaki and A. Takasaki, *Solid State Ionics*, 2016, **298**, 66–72.
26 C. Abughayada, B. Dabrowski, S. Remsen, S. Kolesnik and O. Chmaissem, *J. Solid State Chem.*, 2014, **217**, 127–135.
27 A. Smith, A. Sleight and M. Subramanian, *Mater. Res. Bull.*, 2011, **46**, 1–5.
28 S. Ishiwata, Y. Tokunaga, Y. Taguchi and Y. Tokura, *J. Am. Chem. Soc.*, 2011, **133**, 13818–13820.
29 K. Uusi-Esko and M. Karppinen, *Chem. Mater.*, 2001, **23**, 1835–1840.
30 H. W. Brinks, H. Fjellvåg and A. Kjekshus, *J. Solid State Chem.*, 1997, **129**, 334–340.
31 S. Remsen, B. Dabrowski, O. Chmaissem, J. Mais and A. Szewczyk, *J. Solid State Chem.*, 2011, **184**, 2306–2314.
32 F. M. F. de Groot, J. C. Fuggle, B. T. Thole and G. A. Sawatzky, *Phys. Rev. B: Condens. Matter Mater. Phys.*, 1990, **42**, 5459–5468.
33 G. van der Laan and I. W. Kirkman, *J. Phys.: Condens. Matter*, 1992, **4**, 4189–4204.
34 A. C. Larson and R. B. von Dreele, *Los Alamos Natl. Lab. Rep. – LAUR*, 2004, 86–748.
35 H. B. Toby, *J. Appl. Crystallogr.*, 2001, **34**, 210–213.
36 T. Motohashi, T. Ueda, Y. Masubuchi and S. Kikkawa, *J. Phys. Chem. C*, 2013, **117**, 12560–12566.
37 J. D. Hancock and J. H. Sharp, *J. Am. Ceram. Soc.*, 1972, **55**, 74–77.
38 C. Mitra, Z. Hu, P. Raychaudhuri, S. Wirth, S. I. Csiszar, H. H. Hsieh, H.-J. Lin, C. T. Chen and L. H. Tjeng, *Phys. Rev. B: Condens. Matter Mater. Phys.*, 2003, **67**, 92404.
39 P. Ghigna, A. Campana, A. Lascialfari, A. Caneschi, D. Gatteschi, A. Tagliaferri and F. Borgatti, *Phys. Rev. B: Condens. Matter Mater. Phys.*, 2001, **64**, 132413.